

**Diffusivities and Viscosities of Poly(ethylene oxide)  
Oligomers**

Journal:	<i>Journal of Chemical &amp; Engineering Data</i>
Manuscript ID:	je-2010-00430q
Manuscript Type:	Article
Date Submitted by the Author:	27-Apr-2010
Complete List of Authors:	Hong, Bingbing; Princeton University, Chemical Engineering Escobedo, Fernando; Cornell University, Chemical & Biomolecular Engineering Panagiotopoulos, Athanassios; Princeton University, Chemical Engineering



## Diffusivities and Viscosities of Poly(ethylene oxide) Oligomers

Bingbing Hong<sup>a</sup>, Fernando Escobedo<sup>b</sup>, Athanassios Z. Panagiotopoulos<sup>a\*</sup>

<sup>a</sup>Department of Chemical Engineering, Princeton University, Princeton, New Jersey 08544, USA

<sup>b</sup>School of Chemical and Biomolecular Engineering, Cornell University, Ithaca, New York 14853, USA

### Abstract

Diffusivities and viscosities of poly(ethylene oxide) (PEO) oligomer melts of 1 to 12 repeat units have been obtained from equilibrium molecular dynamics simulations using the TraPPE-UA force field. The simulations generate diffusion coefficients with high accuracy for all molecular weights studied, but statistical uncertainties for the viscosity calculations significantly increase for longer chains. There is in good agreement of calculated viscosities and densities with available experimental data. The simulations can be used to fill in gaps in the data and for extrapolations with respect to chain length, temperature and pressure. We have explored the convergence characteristics of the Green-Kubo formulae for different chain lengths and propose minimal production times required for convergence of the transport properties. The chain length dependence of transport properties suggests that neither Rouse nor reptation models are applicable in the short-chain regime investigated.

---

\* Author for correspondence. Electronic mail: [azp@princeton.edu](mailto:azp@princeton.edu)

## 1. Introduction

Poly(ethylene oxide) (PEO) oligomers have applications as surfactants<sup>1</sup>, polymer electrolytes<sup>2</sup>, and as drug delivery carriers in medical and biological areas<sup>3</sup>. They are also frequently used as model systems in connecting theories and experiments in polymer physics<sup>4,5</sup>. Recently, two new classes of novel hybrid materials have been developed, nanoparticle ionic materials (NIMs)<sup>6,7</sup> and nanoparticle organic hybrid materials (NOHMs)<sup>8</sup>, in which the repeating ‘oxyethylene’ structures form an important component of these materials and contribute to their unique dynamic and transport properties. Establishment of accurate structure-property relations of pure PEO forms the basis for development of new composites in which PEO or its oligomers are a major constituent.

During the past decade, molecular simulations have been frequently used to model PEO chains. Different force fields have been studied, including those based on quantum chemistry<sup>9</sup>, OPLS<sup>10</sup>, and TraPPE and its variations<sup>11-13</sup>. Prior studies have reported a good agreement between simulation predictions and experiments for conformer populations<sup>10,11,14</sup>, spectra<sup>15-17</sup>, thermodynamic properties<sup>12,13,18</sup> and structural relaxations<sup>9,19</sup>. While many atomistic simulations have investigated monodisperse PEO melts of low to moderate molecular weight, there are relatively few studies of higher molecular weight PEO as polydisperse mixtures<sup>13</sup> or in solution<sup>20</sup>. Structural properties and diffusivities of aqueous PEO mixtures are also frequently studied to test transferability of force fields and coarse-graining techniques.<sup>11,21-23</sup>

In contrast to the extensive investigations of static properties, studies of PEO chain dynamics

1  
2  
3  
4 are generally limited by the long time necessary for motion decorrelation at longer length scales.  
5  
6  
7 Dynamic properties explored most frequently are the local correlations of bond, segmental and  
8  
9 sub-chain motions, which relax at time scales of 10ps ~ 100ps.<sup>9, 11, 13, 16, 18, 19</sup> Prior diffusivity  
10  
11 calculations have been limited to melts of short chains or aqueous solutions of oligomers<sup>5, 9, 11</sup>  
12  
13 because diffusivity relates to the slower dynamics of the whole chains. Few studies have looked  
14  
15 into properties of long PEO chains in the bulk<sup>13</sup>. As a property determined by collective chain  
16  
17 motions, viscosity has been even less explored in atomistic models, with values reported only at a  
18  
19 few state points for 12-mers<sup>9</sup>. It is thus worthwhile to use current force fields to obtain systematic  
20  
21 information of transport properties for PEO, especially the dependence on chain length, despite  
22  
23 the need of considerably long simulation times.  
24  
25  
26  
27  
28  
29

30  
31 Transport coefficients can be obtained through either equilibrium methods which use  
32  
33 fluctuation-dissipation formulas or non-equilibrium methods which measure the response of the  
34  
35 system to external perturbations.<sup>24-26</sup> Equilibrium methods are free from theoretical and  
36  
37 practical issues affecting non-equilibrium methods, such as temperature inhomogeneities induced  
38  
39 by the perturbation<sup>27</sup>, and the validity of extrapolation schemes to the equilibrium state<sup>28</sup>. On the  
40  
41 other hand, equilibrium methods have convergence problems if applied to systems characterized  
42  
43 by slow relaxations. Previous papers either reported successful application of Green-Kubo (GK)  
44  
45 formalism to simple systems<sup>29-33</sup> or merely stated qualitatively the difficulty of converging the  
46  
47 GK integrals for large molecules<sup>24, 25, 34</sup>. They have not explored quantitatively the limits of  
48  
49 convergence for chains as a function of their length.  
50  
51  
52  
53  
54  
55

56  
57 In this paper, the TraPPE-UA force field<sup>35, 36</sup> with a corrected dihedral potential<sup>11, 37</sup> is  
58  
59  
60

1  
2  
3  
4 chosen to simulate  $\text{CH}_3\text{O}(\text{CH}_2\text{CH}_2\text{O})_n\text{CH}_3$  for chains of length  $n$  from 1 to 12. Diffusion  
5  
6  
7 coefficients and viscosities are obtained from equilibrium methods. This study provides a test of  
8  
9  
10 the applicability of the TraPPE force field, originally parameterized with phase-equilibrium  
11  
12 properties of small molecules, to transport properties of chains. Unlike previous simulation  
13  
14 studies<sup>9, 11, 13</sup> which have reported viscosity data for a single chain length or diffusivity for low  
15  
16  
17 molecular weight chains, here we systematically study the length dependence of both transport  
18  
19  
20 properties. In addition, we seek to quantify the GK integration divergence for longer chains from  
21  
22  
23 the relative errors of the calculated transport properties.

24  
25 The paper is organized as follows. Section 2 describes the model details and simulation  
26  
27 methodology. Section 3 presents the calculated volumetric and transport properties as functions  
28  
29  
30 of chain length, and compares the results with experimental data and theoretical predictions. The  
31  
32  
33 feasibility of transport property calculations using GK methods for longer chains is also discussed  
34  
35  
36 in the same section. Finally, Section 4 summarizes the conclusions from this work.

## 37 38 39 40 41 **2. Methods**

### 42 43 44 **2.1 Simulation Details and Potential Models**

45  
46  
47 All simulations were performed using GROMACS version 4.0.3<sup>38</sup>. Each  $\text{CH}_3\text{O}(\text{CH}_2\text{CH}_2\text{O})_n\text{CH}_3$   
48  
49  
50 system with  $n$  from 1 to 12 was simulated in the NPT ensemble at pressures of 0, 1 or 10 bar for  
51  
52  
53 an initial simulation time of 3 to 18ns, depending on the chain length. Strictly speaking, zero  
54  
55  
56 pressure corresponds to a metastable liquid, but for liquids away from the critical point the  
57  
58  
59  
60

1  
2  
3  
4 difference in density of the liquid at the saturation (vapor) pressure and at zero pressure is  
5  
6 negligible and simulated systems started from liquid densities never vaporize. The density  
7  
8 averaged over the last 1/3 of each simulation was compared to experimental values, as a measure  
9  
10 of accuracy for the chosen force field. Each system was then reset at the experimental density  
11  
12 (except for 12-mers) and simulations in the NVT ensemble were performed for transport property  
13  
14 calculations with equilibration times from 1 to 120ns and production times from 2 to 40ns, with  
15  
16 longer simulations used for higher molecular weights. Table 1 gives the input parameters for the  
17  
18 simulations, namely, number of chains ( $N$ ), compressibility ( $\kappa_T$ ) used for the barostat in the NPT  
19  
20 runs, and simulation box size ( $L$ ) for the NVT runs for each chain length studied.  
21  
22  
23  
24  
25  
26  
27

28 The configurations were updated via the leap-frog algorithm<sup>39</sup> using a time step of 2fs.  
29  
30 System pressure was coupled to a Parrinello-Rahman barostat<sup>40,41</sup>, with a relaxation time of 5ps  
31  
32 and the compressibilities for different chain systems were set as shown in Table 1. The  
33  
34 Nosé-Hoover thermostat<sup>42,43</sup> was used with a relaxation time of 2.5ps to maintain the system at  
35  
36 temperatures around 300K. Interpolation between experimental melting points of long PEO  
37  
38 chains<sup>44</sup> and oligomers ( $n \leq 4$ )<sup>45</sup> suggests a melting point a little below 300K for the chain lengths  
39  
40 covered in our simulations. Hence, assuming that the force fields we use give melting points not  
41  
42 far away from the corresponding experimental values, all simulated systems are in the stable  
43  
44 liquid region.  
45  
46  
47  
48  
49  
50

51  
52 Interactions between the three types of united atoms in the chains, i.e. CH<sub>3</sub>, CH<sub>2</sub> and O, were  
53  
54 described by the TraPPE-UA force field<sup>35,36</sup>, a set of transferable potentials developed via fitting  
55  
56 to the liquid-vapor coexistence curve of pure substances. Non-bonded interactions in TraPPE-UA  
57  
58  
59  
60

1  
2  
3  
4 include pairwise Lennard-Jones (LJ) and Coulombic potentials. The like-pair LJ diameters and  
5  
6 well depths were  $\sigma(\text{CH}_3) = 3.75\text{\AA}$ ,  $\sigma(\text{CH}_2) = 3.95\text{\AA}$ ,  $\sigma(\text{O}) = 2.80\text{\AA}$  and  $\varepsilon(\text{CH}_3) = 0.8148\text{kJ/mol}$ ,  
7  
8  $\varepsilon(\text{CH}_2) = 0.3825\text{kJ/mol}$ ,  $\varepsilon(\text{O}) = 0.4593\text{kJ/mol}$ , respectively. Unlike-pair interaction parameters  
9  
10 were obtained from the Lorentz-Berthelot combining rules<sup>26</sup> (arithmetic mean for the diameters  
11  
12 and geometric mean for the well depths). Partial charges of  $0.25e$ ,  $0.25e$  and  $-0.50e$  were used for  
13  
14 the  $\text{CH}_3$ ,  $\text{CH}_2$  and  $\text{O}$  centers, respectively. Both van de Waals and electrostatic interactions were  
15  
16 truncated at  $0.9\text{nm}$ . The LJ interactions within the cutoff were determined between a central atom  
17  
18 and the atoms stored in a Verlet neighbor list which is updated every  $10\text{fs}$ , while long-tail  
19  
20 dispersion corrections were treated analytically<sup>26</sup>. The long-range electrostatics are calculated via  
21  
22 the Particle-mesh Ewald method<sup>46, 47</sup> using fourth order interpolation and a Fourier grid spacing  
23  
24 of  $0.12\text{nm}$ . Non-bonded interactions between beads separated by 3 or fewer bonds within one  
25  
26 molecule are not present, as these effects have been incorporated into the angle and torsional  
27  
28 potential parameters. Bond lengths were fixed at  $1.54\text{\AA}$  for  $\text{CH}_x\text{-CH}_y$  ( $x, y = 2, 3$ ) and  $1.41\text{\AA}$  for  
29  
30  $\text{CH}_x\text{-O}$  by the SHAKE algorithm with a relative tolerance of  $10^{-4}$ . Harmonic bond bending  
31  
32 potentials were modeled as  $u_{ijk} = k_\theta(\theta_{ijk} - \theta_0)^2$ , where  $\theta_{ijk}$  is the angle between the 3 consecutive  
33  
34 atoms along two bonds. The force constant  $k_\theta$  and the equilibrium angle  $\theta_0$  were  $k_\theta =$   
35  
36  $502.194\text{kJ/mol}$ ,  $\theta_0 = 112^\circ$  for  $\text{CH}_x\text{-O-CH}_y$  and  $k_\theta = 418.218\text{kJ/mol}$ ,  $\theta_0 = 112^\circ$  for  $\text{CH}_x\text{-CH}_y\text{-O}$ .  
37  
38  
39  
40  
41  
42  
43  
44  
45  
46  
47  
48

49 Fischer et al<sup>11, 37</sup> suggested a modification of torsional potentials in TraPPE-UA force field  
50  
51 in order to match the conformer population distribution with *ab initio* data for  
52  
53 1,2-dimethoxyethane (DME,  $n = 1$ ). The modified TraPPE potential uses Eq. (1)  
54  
55  
56  
57  
58  
59  
60

$$u_{torsion}(\phi) = \sum_{i=0}^7 k_i [1 + \cos(i\phi)] \quad (1)$$

as the new torsion potential function with the parameters listed in Table 2. For small molecules, e.g. DME, TraPPE and modified TraPPE are approximately equivalent with respect to the experimental liquid-vapor coexistence curves: in the temperature range of available experimental data<sup>48</sup>, the original TraPPE force field overestimates the saturated liquid density of DME by 1~2%<sup>36</sup> while the modified TraPPE underestimates it by around 2%<sup>11,49</sup>. Differences between the two force fields increase with the number of  $-\text{CH}_2\text{CH}_2\text{O}-$  units.

Figure 1 presents our results for the  $\rho$ - $P$ - $T$  relationship of dodecaethylene glycol dimethyl ether ( $n = 12$ ,  $(\text{EO})_{12}\text{DME}$ ) at 0 and 1000 bar using both force fields. The simulation statistical uncertainties (error bars), obtained from dividing the samples at each state point into 10 blocks, are smaller than the symbols. Also included in Figure 1 are the experimentally measured curves<sup>50</sup> for poly(ethylene oxide) dimethyl ether (PEODME) mixtures with  $M_n \sim 600$ . The data are better reproduced by the modified TraPPE potential over the entire temperature range at both pressures. Experimental data at 1 bar<sup>9</sup> for PEODME with  $M_n \sim 398$  are represented by triangles in Figure 1; these should have negligible differences from data at 0 bar due to the small compressibility. The system we simulated consists of monodisperse chains having a molecular weight between the  $M_n$ 's of the two experimental systems. We thus confirm that the modified TraPPE force field better reproduces volumetric properties of PEO and we employ it in the following simulations of transport properties.

## 2.2 Diffusivity and Viscosity Calculations

The diffusion coefficient can be obtained by two equivalent equilibrium methods<sup>26</sup>. The Green-Kubo (GK) integration over the velocity autocorrelation function is:

$$D = \frac{1}{3} \int_0^{\infty} \langle \mathbf{v}_i(t+t_0) \cdot \mathbf{v}_i(t_0) \rangle dt \quad (2)$$

In the Einstein relation, the diffusion coefficient is related to the slope of mean square displacement (MSD) of one particle over time:

$$D = \frac{1}{6} \lim_{t \rightarrow \infty} \frac{d}{dt} \langle (\mathbf{r}_i(t+t_0) - \mathbf{r}_i(t_0))^2 \rangle \quad (3)$$

$\mathbf{r}_i(t)$  is the coordinate of center of mass of  $i^{\text{th}}$  molecule at time  $t$ . Averages in Eqs. (2) and (3) are over different time origins and particles in the system. To fully capture the shape of this correlation function from our simulations, velocity files are stored every 0.1ps if GK integration is used. The sampling frequency can be considerably reduced using Eq. (2) in that the transition from sub-diffusive to diffusive region observed from the MSD is less abrupt than the fluctuation of the velocity autocorrelation function. Center-of-mass positions were sampled every 1ps.

Similarly, equilibrium methods for shear viscosity determination include (1) GK integration over the autocorrelation function of the off-diagonal elements of the pressure tensor  $P_{\alpha\beta}$ ,

$$\eta = \frac{V}{k_B T} \int_0^{\infty} \langle P_{\alpha\beta}(t+t_0) P_{\alpha\beta}(t_0) \rangle dt \quad (4)$$

and (2) mean square displacement of  $L_{\alpha\beta}$ , where  $L_{\alpha\beta}$  is defined as

$$L_{\alpha\beta}(t) = \sum_{i=1}^N r_{i\alpha}(t) p_{i\beta}(t) \quad (5)$$

The average in Eq. (4) is taken over different time origins  $t_0$ . Applied to systems with periodic

1  
2  
3  
4 boundary conditions, the second method needs to be modified to remove discontinuities when a  
5  
6 particle jump across the boundary<sup>51, 52</sup>. Recently, an adaptation<sup>52</sup> of Eq. (5) has been derived and  
7  
8 tested for the systems where all potentials obey the minimum-image convention. Because the  
9  
10 relevant modifications to such a method to handle electrostatic interactions are still unclear, in  
11  
12 this work only the boundary-condition-independent GK integral of Eq. (4) was used. Fully  
13  
14 capturing the fastest vibration mode of the pressure correlation function requires  $P_{\alpha\beta}$  to be  
15  
16 sampled every 0.01ps. To gain higher accuracy, the right-hand side of Eq. (4) was further  
17  
18 averaged over the three off-diagonal elements, since PEO melts are isotropic (isotropy was  
19  
20 confirmed during our simulations).  
21  
22  
23  
24  
25  
26

27  
28 The statistical errors of the quantities in Eqs. (2)-(4) were obtained by dividing the time  
29  
30 origins into  $N_b = 5$  blocks for the diffusion coefficient calculation and  $N_b = 10$  blocks for the  
31  
32 viscosity. For each block  $i$ , we averaged the correlation functions or the MSD over time origins in  
33  
34  $i$  and used Eqs. (2) and (3) to obtain the self-diffusion coefficient or viscosity, denoted as  $x_i$ . The  
35  
36 statistical uncertainties with 95% confidence was then determined from  
37  
38  
39

$$Er = 2 \left( \sum_{i=1}^{N_b} (x_i - x)^2 / N_b (N_b - 1) \right)^{1/2} \quad (6)$$

40  
41 where  $x$  is the mean of the series  $x_i$ .  
42  
43  
44  
45  
46  
47  
48

### 49 50 **2.3 System Size Effects**

51  
52 We performed NPT and NVT simulations on systems with 50 and 400 (EO)<sub>5</sub>DME chains in  
53  
54 addition to the base case of 200-(EO)<sub>5</sub>DME chains. The system sizes and calculated transport  
55  
56  
57  
58  
59  
60

1  
2  
3  
4 properties for all systems studied are shown in Tables 1 and 3, respectively. Statistical  
5  
6 uncertainties for densities, viscosities, and diffusivities tend to decrease with system size.  
7  
8 Differences between calculated values at different sizes are within statistical uncertainties,  
9  
10 indicating that system-size effects on the data presented in this paper are not significant.  
11  
12  
13  
14  
15

### 16 **3. Results and Discussions**

#### 17 18 19 **3.1 Calculation of Transport Properties**

20  
21  
22  
23 As indicated by Eq. (4), viscosity is the value to which the integration converges at infinite time.  
24  
25 The pressure autocorrelation functions were obtained from averaging over different time origins  
26  
27 separated by a 10fs interval. Figure 2 presents the normalized values of  $P_{\alpha\beta}$  ( $\alpha\beta = xy, xz, yz$ )  
28  
29 correlation functions for DME and (EO)<sub>12</sub>DME at  $T = 303.15\text{K}$  at the experimental  $P=10$  bar  
30  
31 densities. The curves representing the three directions have perfect overlap at the scale of the  
32  
33 graph with each other, confirming an isotropic system. Figure 2a gives the autocorrelation  
34  
35 functions at short times. Comparison between the two panels in the figure shows that the fastest  
36  
37 vibration modes last longer than 1ps for DME, but are quickly suppressed for the longer  
38  
39 (EO)<sub>12</sub>DME chains. The difference arises from the fact that the backbone atoms or the shortest  
40  
41 segments, responsible for the fast vibrations in (EO)<sub>12</sub>DME, are connected to longer, more  
42  
43 inertial backbone chains and therefore move less freely. The pressure autocorrelation functions  
44  
45 for the two systems at long times (Figure 2b) behave in opposite ways. For the DME melt, the  
46  
47 vibrations become small after  $\sim 3\text{ps}$  and then fluctuate randomly around zero (blue line). The  
48  
49  
50  
51  
52  
53  
54  
55  
56  
57  
58  
59  
60

1  
2  
3  
4 decay of the correlation function (EO)<sub>12</sub>DME melt (violet line) decays slowly and monotonically,  
5  
6  
7 taking ~ 300ps to reach 1% of the value at  $t = 0$ .  
8

9  
10 The viscosity as a function of integration time is given in Figure 3 for DME and (EO)<sub>12</sub>DME  
11  
12 at the same conditions as for Figure 2. One expects viscosity to converge as the integration time  
13  
14 increases and pressure correlation functions decay. In practice, however, statistical noise in the  
15  
16 long-time tail of the pressure correlation functions (Figure 2b) conceals the decay, leading to  
17  
18 poorly converging integrals. In Figure 3, convergence is indicated by a plateau after the initial  
19  
20 increase of the viscosity curves. The increasing error bars and deviations from the plateau at  
21  
22 longer times for the bottom panel illustrate the poor convergence due to contributions from the  
23  
24 noises at the long-time tails of the correlation functions. A similar behavior was also reported in a  
25  
26 study of viscosity for the LJ liquid and SPC water<sup>24</sup>. Therefore, it is very important to choose a  
27  
28 suitable integration time, which should be long enough to cover the main decay region of  
29  
30 pressure correlation functions but short enough to avoid the onset of divergence.  
31  
32  
33  
34  
35  
36  
37  
38

39 Self-diffusion coefficients were calculated from both GK integral (Eq. (2)) and MSD  
40  
41 method (Eq. (3)). Figure 4 gives the results for DME at 303.15K and with a density  
42  
43 corresponding to 10 bar in experiments. Both the velocity autocorrelation function and MSD are  
44  
45 averaged over time origins separated by 1ps intervals, but the velocity files are stored every 0.1ps  
46  
47 in order to record precisely the initial decay of the correlation function. Consequently, MSD  
48  
49 method used 10 times less disk space than the GK integral, although the two methods are  
50  
51 mathematically equivalent and the derivative curve of  $\text{MSD} \sim t$  is expected to match integration  
52  
53 of the velocity autocorrelation function. On the other hand, the GK method applied to diffusivity  
54  
55  
56  
57  
58  
59  
60

1  
2  
3  
4 calculations has considerably better convergence (shown by the negligible error bars in upper  
5  
6 panel of Figure 4) than its application to viscosity calculations (integration over pressure  
7  
8 correlation function). This is because  $D$  is a one-particle property and the average of the velocity  
9  
10 autocorrelation function in Eq. (2) is performed not only over time origins but also over all  
11  
12 molecules involved. For DME, the GK integration can be stopped at around 7ps, at which point  
13  
14 the sub-diffusive regime ends, but the MSD has to be recorded well beyond 7ps until the slope of  
15  
16 the diffusive regime is properly measured. Thus, the GK integral is preferred over the MSD  
17  
18 method in terms of computing time economy.  
19  
20  
21  
22  
23  
24

25 We summarize the data obtained for density, viscosity and diffusivity of different chain  
26  
27 lengths in Table 3. The volumetric data, as also suggested by previous studies that covered a  
28  
29 narrower range of chain lengths and conditions<sup>11, 13, 36</sup>, are in excellent agreement with available  
30  
31 experimental data. For short chains, for which good sampling is easy to obtain, simulated  
32  
33 viscosities match experiments quite well. For longer chains, the relaxation modes in pressure  
34  
35 autocorrelation functions that correspond to whole molecule motions decay slowly and become  
36  
37 sensitive to fluctuations arising from insufficient sampling. Consequently, the errors of simulated  
38  
39 viscosities increase dramatically with chain length. For the longest chain (EO)<sub>12</sub>DME, the  
40  
41 production period was extended to 40ns to diminish fluctuations, but results still have 40%~50%  
42  
43 uncertainties. Much longer simulations would have to be used to obtain significantly more  
44  
45 accurate predictions. For even longer chains, the simulation time necessary for good sampling  
46  
47 becomes prohibitive given current computational resources. The table also suggests that current  
48  
49 equilibrium-based atomistic simulations are likely only feasible for viscosity calculations in  
50  
51  
52  
53  
54  
55  
56  
57  
58  
59  
60

1  
2  
3  
4 systems no more viscous than  $\sim 100$ cP. The relation between uncertainties and simulation time is  
5  
6 discussed in Sec. 3.3.  
7

8  
9 Experimental self-diffusion coefficients for  $\text{CH}_3\text{O}(\text{CH}_2\text{CH}_2\text{O})_n\text{CH}_3$  are not currently  
10  
11 available for  $n > 2$ . Based on the agreement of the calculated diffusivity for DME with  
12  
13 experimental measurements and the good match between mean values of viscosity and the  
14  
15 experiments, our calculations for the diffusivities of longer chains can be considered as  
16  
17 predictions to be validated by future experiments. The results also indicate that the modified  
18  
19 TraPPE is a force field of good quality, giving excellent agreement with experimental data not  
20  
21 only for the thermodynamic properties for which it was optimized, but also for transport  
22  
23 properties.  
24  
25  
26  
27  
28  
29  
30  
31

### 32 **3.2 Scaling Laws**

33  
34  
35

36 Our results for viscosities and diffusivities of the PEO chains are plotted as functions of chain  
37  
38 length in Figures 5 and 6. The viscosity scales with chain length with exponents between 1.5 ~  
39  
40 2.4; the diffusivity scales as  $-1.9 \sim -2.5$ . In polymer theories, unentangled and entangled chain  
41  
42 dynamics are usually described by the Rouse and reptation models, respectively, which give:  $D \sim$   
43  
44  $M^{-1}$ ,  $\eta \sim M^1$  for  $M < M_c$ ;  $D \sim M^{-2}$ ,  $\eta \sim M^{3.3 \sim 3.4}$  for  $M > M_c$ , where  $M_c$  is the critical molecular  
45  
46 weight beyond which the entanglements take effect<sup>53</sup>. The scaling exponent for viscosity is thus  
47  
48 between the predicted values before and after entanglements. The relation  $\eta \sim M^1$  (Rouse model)  
49  
50 describes a melt of ideal chains, whereas in our simulations and experiments the chains are driven  
51  
52 away from ideal configurations by not only bonded interactions (the angle and torsional  
53  
54  
55  
56  
57  
58  
59  
60

1  
2  
3  
4 potentials) which bring in stiffness, but also the non-bonded interactions that prevent the chains  
5  
6 from crossing each other. These interactions slow down the chain motions, resulting in a more  
7  
8 viscous system. However, limits imposed from such interactions on chain motions are still  
9  
10 smaller than that of long-chain entanglements. The entanglements, as described by the reptation  
11  
12 model, reduce the chain motions to one-dimensional movements along its contour, whereas  
13  
14 non-bonded interactions alone still allow chains to have freedom to move laterally. The  
15  
16 difference explains the smaller simulated exponent compared with the reptation model prediction.  
17  
18 The scaling exponent for the self-diffusion coefficient is almost the same as that of the reptation  
19  
20 model.  
21  
22  
23  
24  
25  
26

27  
28 We have included in Figures 5 and 6 experimental data for liquid *n*-alkanes with *n* from 4 to  
29  
30 18. The viscosities and diffusivities of *n*-alkanes scale in a similar fashion to PEO oligomers. The  
31  
32 closeness of the slopes suggests that inter- and intra-molecular interactions play a similar role in  
33  
34 these oligomers. Previous simulations of fully flexible Lennard-Jones generated scaling factors  
35  
36 ( $D \sim n^{-0.8 \sim -0.5}$  and  $\eta \sim n^{0.6 \sim 0.7}$ )<sup>54, 55</sup> significantly different from this paper, suggesting an  
37  
38 important but still unclear effect from the chain stiffness onto the scaling behaviors of short  
39  
40 chains.. Although the reported exponents are obtained from a series of chains applied by constant  
41  
42 density condition and the chains of different lengths in the paper are set at the densities  
43  
44 determined by fixed pressure, it seems unlikely for the two sets of exponent ranges to overlap  
45  
46 even if the values of LJ chains are converted to fixed pressure condition. For *n*-alkanes, it is  
47  
48 known that the crossover to ideal chain statistics takes place when number of methylenes is  
49  
50 greater than 100<sup>56, 57</sup>. With stronger electrostatic interactions, PEO chains are expected to be  
51  
52  
53  
54  
55  
56  
57  
58  
59  
60

1  
2  
3  
4 stiffer. As a result, PEO needs more backbone repeat units than  $n$ -alkanes to have an  
5  
6 independent-rotating segment and enter the Gaussian-chain regime. The critical length of a  
7  
8 polymer for the entanglement to take effect, however, depends in a non-trivial way on backbone  
9  
10 stiffness. Chain stiffness has been shown to accelerate the onset of reptation regime for LJ  
11  
12 chains<sup>58</sup>. It would be interesting to test if that counter-intuitive relation between stiffness and  
13  
14 entanglement length remains true for PEO and  $n$ -alkanes chains of longer length.  
15  
16  
17  
18  
19

### 20 21 **3.3 Convergence of Transport Properties**

22  
23  
24  
25 In Sec. 3.1, we stated that the integration time in Eq. (4) needs to be suitably chosen in order to  
26  
27 cover the main relaxation region of pressure correlation functions and avoid the divergence  
28  
29 region (large errors or deviation from the plateau). It has also been pointed out that insufficient  
30  
31 sampling brings large fluctuations into the long-tail decay part and leads to early divergence of  
32  
33 the integration. How can we determine whether the sampling is sufficient and whether the  
34  
35 integration time is neither too long nor too short? There should be a relation between integration  
36  
37 time, number of samples, and the quantity measuring the degree of divergence.  
38  
39  
40  
41  
42  
43

44 We introduce for the pressure correlation function a relaxation time  $\tau$ , defined as the time  $t_0$   
45  
46 +  $\tau$  at which the long-tail normalized correlation function is reduced to 0.1% of the value at  $t_0$ .  
47  
48 The relaxation times for chains with  $n = 1, 3, 5, 9, 12$  are obtained from our simulations as 3ps,  
49  
50 15ps, 50ps, 200ps and 500ps respectively. The degree of divergence of the integration is  
51  
52 measured by the relative error, which is defined as the ratio of the statistical uncertainty of a  
53  
54 quantity to its mean value. If we set the integration time  $t_{int} = 10\tau$ , Figure 7 presents the relation  
55  
56  
57  
58  
59  
60

1  
2  
3  
4 between the relative error and the number of samples obtained at  $t_{ill}$ . Results from both pentamer  
5  
6 and dodecamer indicate a quick drop of relative error with increasing number of samples when  
7  
8 the sample number is still small. Once the relative error gets to around 50%, the convergence of  
9  
10 the GK integration can not be improved as effectively by additional sampling as before. This  
11  
12 flattening tendency reveals the computational difficulty of realizing better convergence (e.g.  
13  
14 <30% relative error) especially for long chains.  
15  
16  
17  
18  
19

20 If we set 60% relative error to be the point separating convergence and divergence (any  
21  
22 choice in the 50 ~ 80% range would give similar conclusions), the rough number of samples  
23  
24 necessary for the GK integral to be convergent is shown in Figure 8 as a function of chain length.  
25  
26 The number of samples can be considered to be roughly proportional to CPU time and therefore  
27  
28 it is an indirect measure of the minimal production time needed to converge the GK integral,  $t_m$ .  
29  
30 Fitting the data in Figure 8 gives  $t_m \sim N^\alpha$  with  $\alpha \approx 1.2$  at the short-chain end and  $\alpha \approx 2.4$  when  $N$   
31  
32 approaches 12. The exponents are very close to those for the  $\tau \sim N^\beta$  relation where  $\tau$  is the  
33  
34 relaxation time of the pressure autocorrelation function defined before and  $\beta \approx 1.7 \sim 2.6$  when  $N$   
35  
36 goes from  $n = 1$  to 12. The time  $\tau$  can also be viewed as being roughly proportional to the time  
37  
38 to fully equilibrate the chain melts. Assuming a characteristic monomer relaxation time of  
39  
40  $\sim 10^{-10}$ s,<sup>16</sup> the relaxation time for (EO)<sub>12</sub>DME is  $\sim 80$ ns, confirming that our simulations are  
41  
42 long enough.  
43  
44  
45  
46  
47  
48  
49  
50

51 In Reference 26, a relation was derived for the standard error of the normalized correlation  
52  
53 function in the form of  $t_{run}^{-1/2}$ , where  $t_{run}$  is the length of production time. This scaling provides an  
54  
55 alternative to estimate the minimal run length in order to reduce noise in correlation functions. It  
56  
57  
58  
59  
60

1  
2  
3  
4 is applicable to different correlation functions and easy to use for quick estimations with any new  
5  
6 system. However, the errors in the transport properties originate from two factors – correlation  
7  
8 function calculation and integration. The method of Ref. 26 leaves the second factor unaddressed.  
9  
10  
11 On the contrary, though the scaling relations obtained in this paper are confined to the PEO melt  
12  
13 system, they take into account both factors and relate the final degree of divergence directly to  
14  
15 run length.  
16  
17  
18  
19

#### 20 21 **4. Conclusions**

22  
23  
24  
25 Atomistic molecular dynamics simulations have been carried out, using the modified TraPPE-UA  
26  
27 force field, to investigate the transport properties of PEO oligomers, specifically  
28  
29  $\text{CH}_3\text{O}(\text{CH}_2\text{CH}_2\text{O})_n\text{CH}_3$  with  $1 \leq n \leq 12$ . We have demonstrated that transport properties for this  
30  
31 class of molecules can be obtained from equilibrium molecular dynamics simulations. As a  
32  
33 single-particle property, diffusivity is calculated with a fast convergence and high accuracy for all  
34  
35 chain lengths of interest using the Green-Kubo formula. Viscosities, however, are less  
36  
37 satisfactorily determined via the Green-Kubo integral due to significant sampling difficulties.  
38  
39 Although the method can be used for short chains, insufficient sampling for the pressure  
40  
41 autocorrelation functions results in a poor GK integral convergence. The method is not suitable  
42  
43 for viscosity calculations of chains longer than the ones studied here.  
44  
45  
46  
47  
48  
49  
50

51  
52 Through the exploration into how sampling affects the convergence or relative errors, we  
53  
54 obtain a rough relation estimating the minimal production time necessary for relative errors under  
55  
56 a given tolerance as a function of chain length. We also obtained a relation between equilibrium  
57  
58  
59  
60

1  
2  
3  
4 (pre-production) time and chain length, which enabled us to ensure that the systems had been  
5  
6 fully equilibrated before the properties of interest were sampled, an issue that most prior studies  
7  
8 did not address<sup>9, 11, 13, 31, 57</sup>. The methodology proposed here to estimate the simulation time for  
9  
10 long chains based on the scaling relation of short chains, can be extended to other polymer  
11  
12 systems. It gives useful information to assess when the equilibrium methods are effective, when  
13  
14 they break down, and how much additional computational efforts may be required to improve  
15  
16 predictions.  
17  
18  
19  
20  
21

22  
23 No prior systematic investigations of viscosity or diffusivity in the melt had been performed  
24  
25 for PEO chains. This work obtained the chain-length dependence of viscosity and diffusivity for  
26  
27 PEO oligomers and compared it to experiments and to the behavior of *n*-alkanes. The similar  
28  
29 scaling factors of the two systems reflect the influences of intra- and inter-molecular interactions  
30  
31 on the dynamics of these oligomers. Compared to the Rouse and reptation models, the exponents  
32  
33 also suggest chain lengths of interest in the paper are far from ideal-chain statistics and the region  
34  
35 where entanglements take effect. Finally, our simulations confirm the applicability of the  
36  
37 TraPPE-based force field, which has been widely tested for structural and thermodynamic  
38  
39 properties, to transport properties of PEO melts.  
40  
41  
42  
43  
44  
45  
46  
47

## 48 **Acknowledgements**

49  
50 This publication is based on work supported by Award No. KUS-CI-018-02 made by King  
51  
52 Abdullah University of Science and Technology (KAUST). This paper is dedicated to Sir John  
53  
54 Rowlinson or his many contributions to experiment, theory and history of thermodynamics and  
55  
56  
57  
58  
59  
60

1  
2  
3  
4 for his mentorship of one of us (AZP) at a critical and formative time.  
5  
6  
7  
8  
9  
10

## 11 12 **References**

- 13  
14  
15 1. Drohmann, C.; Beckman, E. J., Phase behavior of polymers containing ether groups in  
16 carbon dioxide. *J. Supercrit. Fluids* **2002**, 22, 103-110.  
17  
18
- 19  
20 2. Croce, F.; Appetecchi, G. B.; Persi, L.; Scrosati, B., Nanocomposite polymer electrolytes for  
21 lithium batteries. *Nature* **1998**, 394, 456-458.  
22  
23
- 24  
25 3. Harris, J. M., *Poly(ethylene glycol) Chemistry: Biotechnological and Biomedical*  
26 *Applications*. Plenum Press: New York, 1992.  
27  
28
- 29  
30 4. Teramoto, A.; Fujita, H., Temperature and Molecular Weight Dependence of Melt Viscosity  
31 of Polyethylene Oxide in Bulk. *Makromol. Chem.* **1965**, 85, 261-272.  
32  
33
- 34  
35 5. Shimada, K.; Kato, H.; Saito, T.; Matsuyama, S.; Kinugasa, S., Precise measurement of the  
36 self-diffusion coefficient for poly(ethylene glycol) in aqueous solution using uniform oligomers.  
37 *J. Chem. Phys.* **2005**, 122, S4035-S4046.  
38  
39
- 40  
41 6. Bourlinos, A. B.; Giannelis, E. P.; Zhang, Q.; Archer, L. A.; Floudas, G.; Fytas, G.,  
42 Surface-functionalized nanoparticles with liquid-like behavior: The role of the constituent  
43 components. *European Physical Journal E* **2006**, 20, 109-117.  
44  
45
- 46  
47 7. Rodriguez, R.; Herrera, R.; Archer, L. A.; Giannelis, E. P., Nanoscale Ionic Materials. *Adv.*  
48 *Mater. (Weinheim, Ger.)* **2008**, 20, 4353-4358.  
49  
50
- 51  
52 8. Qi, H.; Agarwal, P.; Archer, L. A., Time-strain superposition in suspensions of hairy  
53 nanoparticles. *submitted*.  
54  
55
- 56  
57 9. Borodin, O.; Douglas, R.; Smith, G. A.; Trouw, F.; Petrucci, S., MD Simulations and  
58 experimental study of structure, dynamics, and thermodynamics of poly(ethylene oxide) and its  
59  
60

1  
2  
3 oligomers. *J. Phys. Chem. B* **2003**, 107, 6813-6823.  
4  
5

6  
7 10. Anderson, P. M.; Wilson, M. R., Developing a force field for simulation of poly(ethylene  
8 oxide) based upon ab initio calculations of 1,2-dimethoxyethane. *Mol. Phys.* **2005**, 103, 89-97.  
9

10  
11 11. Fischer, J.; Paschek, D.; Geiger, A.; Sadowski, G., Modeling of aqueous poly(oxyethylene)  
12 solutions: 1. Atomistic Simulations. *J. Phys. Chem. B* **2008**, 112, 2388-2398.  
13  
14

15  
16 12. Tritopoulou, E. A.; Economou, I. G., Molecular simulation of structure and thermodynamic  
17 properties of pure tri- and tetra-ethylene glycols and their aqueous mixtures. *Fluid Phase Equilib.*  
18 **2006**, 248, 134-146.  
19

20  
21  
22 13. Wick, C. D.; Theodorou, D. N., Connectivity-altering Monte Carlo Simulations of the end  
23 group effects on volumetric properties for poly(ethylene oxide). *Macromolecules* **2004**, 37,  
24 7026-7033.  
25  
26

27  
28 14. Neyertz, S.; Brown, D.; Thomas, J. O., Molecular-Dynamics Simulation of Crystalline  
29 Poly(Ethylene Oxide). *J. Chem. Phys.* **1994**, 101, 10064-10073.  
30  
31

32  
33 15. Smith, G. D.; Yoon, D. Y.; Jaffe, R. L.; Colby, R. H.; Krishnamoorti, R.; Fetters, L. J.,  
34 Conformations and structures of poly(oxyethylene) melts from molecular dynamics simulations  
35 and small-angle neutron scattering experiments. *Macromolecules* **1996**, 29, 3462-3469.  
36  
37

38  
39 16. Lin, B.; Boinske, P. T.; Halley, J. W., A molecular dynamics model of the amorphous  
40 regions of polyethylene oxide. *J. Chem. Phys.* **1996**, 105, 1668-1681.  
41  
42

43  
44 17. Sasanuma, Y.; Ohta, H.; Touma, I.; Matoba, H.; Hayashi, Y.; Kaito, A., Conformational  
45 characteristics of poly(ethylene sulfide) and poly(ethylene oxide): Solvent dependence of  
46 attractive and repulsive gauche effects. *Macromolecules* **2002**, 35, 3748-3761.  
47  
48

49  
50 18. Neyertz, S.; Brown, D.; Colombini, D.; Alberola, N. D.; Merle, G., Volume dependence of  
51 molecular flexibility in poly(ethylene oxide) under negative pressure. *Macromolecules* **2000**, 33,  
52 1361-1369.  
53  
54

55  
56 19. Neyertz, S.; Brown, D., A Computer-Simulation Study of the Chain Configurations in  
57 Poly(Ethylene Oxide)-Homolog Melts. *J. Chem. Phys.* **1995**, 102, 9725-9735.  
58  
59  
60

- 1  
2  
3  
4  
5  
6  
7  
8  
9  
10  
11  
12  
13  
14  
15  
16  
17  
18  
19  
20  
21  
22  
23  
24  
25  
26  
27  
28  
29  
30  
31  
32  
33  
34  
35  
36  
37  
38  
39  
40  
41  
42  
43  
44  
45  
46  
47  
48  
49  
50  
51  
52  
53  
54  
55  
56  
57  
58  
59  
60
20. Brodeck, M.; Alvarez, F.; Arbe, A.; Juranyi, F.; Unruh, T.; Holderer, O.; Colmenero, J.; Richter, D., Study of the dynamics of poly(ethylene oxide) by combining molecular dynamic simulations and neutron scattering experiments. *J. Chem. Phys.* **2009**, 130, 6319-6326.
21. Shang, B. Z.; Wang, Z. W.; Larson, R. G., Molecular dynamics simulation of interactions between a sodium dodecyl sulfate micelle and a poly(ethylene oxide) polymer. *J. Phys. Chem. B* **2008**, 112, 2888-2900.
22. Smith, G. D.; Bedrov, D., A molecular dynamics simulation study of the influence of hydrogen-bonding and polar interactions on hydration and conformations of a poly(ethylene oxide) oligomer in dilute aqueous solution. *Macromolecules* **2002**, 35, 5712-5719.
23. Smith, G. D.; Borodin, O.; Bedrov, D., A revised quantum chemistry-based potential for poly(ethylene oxide) and its oligomers in aqueous solution. *J. Comput. Chem.* **2002**, 23, 1480-1488.
24. Hess, B., Determining the shear viscosity of model liquids from molecular dynamics simulations. *J. Chem. Phys.* **2002**, 116, 209-217.
25. Bordat, P.; Muller-Plathe, F., The shear viscosity of molecular fluids: A calculation by reverse nonequilibrium molecular dynamics. *J. Chem. Phys.* **2002**, 116, 3362-3369.
26. Allen, M. P.; Tildesley, D. J., *Computer Simulation of Liquids*. Oxford University Press Inc.: New York, 1987.
27. Liem, S. Y.; Brown, D.; Clark, J. H. R., Investigation of the homogeneous-shear nonequilibrium-molecular-dynamics methods. *Phys. Rev. A* **1992**, 45, 3706-3713.
28. Travis, K. P.; Searles, D. J.; Evans, D. J., Strain rate dependent properties of a simple fluid. *Mol. Phys.* **1998**, 95, 195-202.
29. Meier, K.; Laesecke, A.; Kabelac, S., Transport coefficients of the lennard-jones model fluid. I. Viscosity. *J. Chem. Phys.* **2004**, 121, 3671-3687.
30. Meier, K.; Laesecke, A.; Kabelac, S., Transport coefficients of the Lennard-Jones model fluid. II Self-diffusion. *J. Chem. Phys.* **2004**, 121, 9526-9535.

- 1  
2  
3  
4  
5  
6  
7  
8  
9  
10  
11  
12  
13  
14  
15  
16  
17  
18  
19  
20  
21  
22  
23  
24  
25  
26  
27  
28  
29  
30  
31  
32  
33  
34  
35  
36  
37  
38  
39  
40  
41  
42  
43  
44  
45  
46  
47  
48  
49  
50  
51  
52  
53  
54  
55  
56  
57  
58  
59  
60
31. Yoo, C. D.; Kim, S.-C.; Lee, S. H., Viscosity and Diffusion of Small Normal and Isomeric Alkanes: An Equilibrium Molecular Dynamics Simulation Study. *Bull. Korean Chem. Soc.* **2008**, 29, 1059-1062.
32. Rey-Castro, C.; Vega, L. F., Transport properties of the ionic liquid 1-ethyl-3-methylimidazolium chloride from equilibrium molecular dynamics simulation. The effect of temperature. *J. Phys. Chem. B* **2006**, 110, 14426-14435.
33. Rey-Castro, C.; Vega, L. F., Transport properties of the ionic liquid 1-ethyl-3-methylimidazolium chloride from equilibrium molecular dynamics simulation. The effect of temperature (vol 110B, pg 14, 2006). *J. Phys. Chem. B* **2006**, 110, 16157-16157.
34. Borodin, O.; Smith, G. D.; Kim, H., Viscosity of a Room Temperature Ionic Liquid: Predictions from Nonequilibrium and Equilibrium Molecular Dynamics Simulations. *J. Phys. Chem. B* **2009**, 113, 4771-4774.
35. Martin, M. G.; Siepmann, J. I., Transferable potentials for phase equilibria. 1. United-atom description of n-alkanes. *J. Phys. Chem. B* **1998**, 102, 2569-2577.
36. Stubbs, J. M.; Potoff, J. J.; Siepmann, J. I., Transferable potentials for phase equilibria. 6. United-atom description for ethers, glycols, ketones, and aldehydes. *J. Phys. Chem. B* **2004**, 108, 17596-17605.
37. Fischer, J.; Paschek, D.; Geiger, A.; Sadowski, G., Modeling of aqueous poly(oxyethylene) solutions: 1. Atomistic simulations (vol 112, pg 2388, 2008). *J. Phys. Chem. B* **2008**, 112, 8849-8850.
38. van der Spoel, D.; Lindahl, E.; Hess, B.; van Buuren, A. R.; Apol, E.; Meulenhoff, P. J.; Tieleman, D. P.; Sijbers, A. L. T. M.; Feenstra, K. A.; van Drunen, R.; Berendsen, H. J. C., Gromacs User Manual version 4.0. In 2005.
39. Hockney, R. W.; Goel, S. P.; Eastwood, J. W., Quiet High-Resolution Computer Models of a Plasma. *J. Comput. Phys.* **1974**, 14, 148-158.
40. Parrinello, M.; Rahman, A., Polymorphic Transitions in Single-Crystals - a New Molecular-Dynamics Method. *J. Appl. Phys.* **1981**, 52, 7182-7190.

- 1  
2  
3 41. Nose, S.; Klein, M. L., Constant Pressure Molecular-Dynamics for Molecular-Systems. *Mol.*  
4 *Phys.* **1983**, 50, 1055-1076.  
5  
6  
7  
8 42. Nose, S., A Molecular-Dynamics Method for Simulations in the Canonical Ensemble. *Mol.*  
9 *Phys.* **1984**, 52, 255-268.  
10  
11  
12 43. Hoover, W. G., Canonical Dynamics - Equilibrium Phase-Space Distributions. *Phys. Rev. A*  
13 **1985**, 31, 1695-1697.  
14  
15  
16  
17 44. Hay, J. N., Equilibrium Melting-Point of Poly(Ethylene Oxide). *Makromolekulare*  
18 *Chemie-Macromol. Chem. Phys.* **1976**, 177, 2559-2561.  
19  
20  
21  
22 45. Linstrom, P. J.; Mallard, W. G., Eds., *NIST Chemistry WebBook, NIST Standard Reference*  
23 *Database Number 69*, National Institute of Standards and Technology: Gaithersburg MD.  
24 (retrieved March 27, 2010) [webbook.nist.gov/chemistry](http://webbook.nist.gov/chemistry)  
25  
26  
27  
28 46. Darden, T.; York, D.; Pedersen, L., Particle Mesh Ewald - an N.Log(N) Method for Ewald  
29 Sums in Large Systems. *J. Chem. Phys.* **1993**, 98, 10089-10092.  
30  
31  
32  
33 47. Essmann, U.; Perera, L.; Berkowitz, M. L.; Darden, T.; Lee, H.; Pedersen, L. G., A Smooth  
34 Particle Mesh Ewald Method. *J. Chem. Phys.* **1995**, 103, 8577-8593.  
35  
36  
37  
38 48. Properties of Organic Compounds. <http://www.chemnetbase.com/scripts/pocweb.exe>  
39  
40  
41 49. Ku, H. C.; Tu, C. H., Densities and viscosities of seven glycol ethers from 288.15 K to  
42 343.15 K. *J. Chem. Eng. Data* **2000**, 45, 391-394.  
43  
44  
45  
46 50. Zoller, P.; Walsh, D. J., *Standard Pressure-Volume-Temperature Data for Polymers*  
47 Technomic Pub. Co.: Lancaster, PA, 1995.  
48  
49  
50  
51 51. Erpenbeck, J. J., Einstein-Kubo-Helfand and Mcquarrie Relations for Transport-Coefficients.  
52 *Phys. Rev. E* **1995**, 51, 4296-4308.  
53  
54  
55 52. Viscardy, S.; Servantie, J.; Gaspard, P., Transport and Helfand moments in the  
56 Lennard-Jones fluid. I. Shear viscosity. *J. Chem. Phys.* **2007**, 126, 184512.  
57  
58  
59  
60

- 1  
2  
3  
4 53. de Gennes, P. G., *Scaling Concepts in Polymer Physics*. Cornell University Press: 1979.
- 5  
6  
7 54. Galliero, G.; Boned, C., Shear viscosity of the Lennard-Jones chain fluid in its gaseous,  
8 supercritical, and liquid states. *Phys. Rev. E* **2009**, 79, 021201.
- 9  
10  
11 55. Reis, R. A.; Silva, F. C.; Nobrega, R.; Oliveira, J. V.; Tavares, F. W., Molecular dynamics  
12 simulation data of self-diffusion coefficient for Lennard-Jones chain fluids. *Fluid Phase Equilib.*  
13 **2004**, 221, 25-33.
- 14  
15  
16  
17 56. Brown, D.; Clarke, J. H. R.; Okuda, M.; Yamazaki, T., A Molecular-Dynamics Study of  
18 Chain Configurations in N-Alkane-Like Liquids. *J. Chem. Phys.* **1994**, 100, 1684-1692.
- 19  
20  
21  
22 57. Lee, S. H.; Chang, T. Y., Viscosity and diffusion constants calculation of n-alkanes by  
23 molecular dynamics simulations. *Bull. Korean Chem. Soc.* **2003**, 24, 1590-1598.
- 24  
25  
26  
27 58. Faller, R.; Muller-Plathe, F., Chain stiffness intensifies the reptation characteristics of  
28 polymer dynamics in the melt. *ChemPhysChem* **2001**, 2, 180-184.
- 29  
30  
31  
32 59. Benson, G. C.; Wang, L. L.; Lu, B. C. Y., Excess enthalpies of (heptane plus methyl  
33 1,1-dimethylethyl ether plus 1,2-dimethoxyethane) at the temperature 298.15 K and ambient  
34 pressure. *J. Chem. Thermodyn.* **1998**, 30, 1533-1541.
- 35  
36  
37  
38 60. Comunas, M. J. P.; Lopez, E. R.; Pires, P.; Garcia, J.; Fernandez, J., p rho T measurements of  
39 polyethylene glycol dimethylethers between 278.15 and 328.15 K at pressures to 12 MPa. *Int. J.*  
40 *Thermophys.* **2000**, 21, 831-851.
- 41  
42  
43  
44 61. Zheng, P. J.; Meng, X. Y.; Wu, J. T.; Liu, Z. G., Density and viscosity measurements of  
45 dimethoxymethane and 1,2-dimethoxyethane from 243 K to 373 K up to 20 MPa. *Int. J.*  
46 *Thermophys.* **2008**, 29, 1244-1256.
- 47  
48  
49  
50 62. Bedrov, D.; Borodin, O.; Smith, G. D.; Trouw, F.; Mayne, C., Simulation and QENS studies  
51 of molecular dynamics in aqueous solutions of 1,2-dimethoxyethane. *J. Phys. Chem. B* **2000**, 104,  
52 5151-5154.
- 53  
54  
55  
56 63. Das, B.; Roy, M. N.; Hazra, D. K., Densities and Viscosities of the Binary Aqueous Mixtures  
57 of Tetrahydrofuran and 1,2-Dimethoxyethane at 198, 308 and 318 K. *Indian J. Chem. Technol.*

1  
2  
3 **1994**, 1, 93-97.  
4

5  
6  
7 64. Kusano, K., Densities, Refractive-Indexes, and Normal Boiling Points of 1,2-Disubstituted  
8 Ethylene-Glycol Derivatives. *J. Chem. Eng. Data* **1978**, 23, 141-143.  
9

10  
11 65. Pal, A.; Sharma, S., Excess molar volumes and viscosities of 1-propanol plus ethylene glycol,  
12 plus ethylene glycol monomethyl, plus ethylene glycol dimethyl, plus diethylene glycol dimethyl,  
13 plus triethylene glycol dimethyl, plus diethylene glycol diethyl, and plus diethylene glycol  
14 dibutyl ethers at 298.15K. *J. Chem. Eng. Data* **1998**, 43, 532-536.  
15  
16

17  
18  
19 66. Ku, H. C.; Tu, C. H., Densities and viscosities of binary and ternary mixtures of ethanol,  
20 2-butanone, and 2,2,4-trimethylperitane at T = (298.15, 308.15, and 318.15) K. *J. Chem. Eng.*  
21 *Data* **2005**, 50, 608-615.  
22  
23

24  
25 67. Conesa, A.; Shen, S.; Coronas, A., Liquid densities, kinematic viscosities, and heat capacities  
26 of some ethylene glycol dimethyl ethers at temperatures from 283.15 to 423.15 K. *Int. J.*  
27 *Thermophys.* **1998**, 19, 1343-1358.  
28  
29

30  
31 68. Lide, D. R. H., WM CRC Handbook of Chemistry and Physics. [www.hbcpnetbase.com](http://www.hbcpnetbase.com)  
32  
33

34  
35 69. Douglass, D. C.; McCall, D. W., Diffusion in Paraffin Hydrocarbons. *J. Phys. Chem.* **1958**,  
36 62, 1102-1107.  
37

38  
39 70. Ertl, H.; Dullien, F. A. L., Self-Diffusion and Viscosity of Some Liquids as a Function of  
40 Temperature. *AIChE J.* **1973**, 19, 1215-1223.  
41  
42  
43  
44  
45  
46  
47  
48  
49  
50  
51  
52  
53  
54  
55  
56  
57  
58  
59  
60

**Table 1.** Simulation parameters

$n$	$N$	$\kappa_T$ ( $10^{-5}\text{bar}^{-1}$ )	$L$ (nm) <sup>d</sup>
1	216	11.15 <sup>59</sup>	3.34570 <sup>a</sup> (296.15K, 1bar)
			3.3390 <sup>a</sup> (298.15K, 1bar)
			3.3534 <sup>a</sup> (303.15K, 10bar)
3	216	7.31 <sup>60</sup>	4.0300 <sup>a</sup> (303.15K, 10bar)
5	50	6.6 <sup>60</sup>	2.7880 <sup>a</sup> (303.15K, 10bar)
			4.4257 <sup>a</sup> (303.15K, 10bar)
			5.5760 <sup>a</sup> (303.15K, 10bar)
9	150	5.5 <sup>c</sup>	4.7070 <sup>a</sup> (303.15K, 10bar)
			4.7114 <sup>a</sup> (318K, 1bar)
12	100	5.0 <sup>c</sup>	4.4819 <sup>b</sup> (298.15K, 1bar)
			4.4672 <sup>b</sup> (303.15K, 10bar)

<sup>a</sup>determined according to experimental density; <sup>b</sup>determined from NPT simulation density;

<sup>c</sup>extrapolated from  $n = 1 \sim 5$ ; <sup>d</sup>the temperature and the pressure followed are the experimental state points at which the density is reached

**Table 2.** Dihedral Parameters in modified TraPPE-UA Force Field

	$k_i/(\text{kJ}\cdot\text{mol}^{-1})$							
	i = 0	1	2	3	4	5	6	7
CH <sub>x</sub> -O-CH <sub>y</sub> -CH <sub>y</sub>	-0.25390	-5.15997	-0.69711	5.35013	0.80312	0.28307	0.09526	-0.05797
O-CH <sub>x</sub> -CH <sub>x</sub> -O	-7.75967	7.58526	6.70523	8.40071	0.63221	0.11063	0.35962	0.01683

**Table 3.** Densities, viscosities and diffusivities of CH<sub>3</sub>O(CH<sub>2</sub>CH<sub>2</sub>O)<sub>n</sub>CH<sub>3</sub> (*n* = 1 ~ 12)

<i>n</i>	State point	Density (g/cm <sup>3</sup> ) <sup>a</sup>		Viscosity (cP)		Diffusivity (10 <sup>-5</sup> cm <sup>2</sup> /s)	
		sim <sup>b</sup>	expr <sup>c</sup>	sim	expr	sim	expr
	296.15K, 1bar	0.852±0.001	0.8631 <sup>61</sup>			3.15±0.02	3.2 <sup>11, 62</sup>
1	298.15K, 1bar	0.8481±0.0008	0.8613 <sup>63</sup> , 0.8637 <sup>64</sup> , 0.8626 <sup>65</sup>	0.35±0.02	0.394 <sup>66</sup>	3.13±0.04	
	303.15K, 10bar	0.843±0.001	0.8518 <sup>67</sup>	0.34±0.07	0.402 <sup>67</sup>	3.47±0.04	
3	303.15K, 10bar	0.968±0.001	0.9768 <sup>67</sup>	1.7±0.4	1.761 <sup>67</sup>	0.61±0.02	
5	303.15K, 10bar	<i>N</i> = 50	1.016±0.002		4.4±3.3		0.15±0.03
		<i>N</i> = 200	1.0155±0.0006	1.0204 <sup>67</sup>	5.0±2.1	4.588 <sup>67</sup>	0.181±0.008
		<i>N</i> = 400	1.0160±0.0003		4.8±2.5		0.187±0.009
9	303.15K, 10bar	1.056±0.001		16.3±9.5		0.041±0.005	
	318K, 1bar	1.0398±0.0006	1.054, 1.048, 1.038 <sup>9</sup>	11.9±7.0	13.34 <sup>9</sup>	0.062±0.005	
12	298.15K, 1bar			33.3±15.0		0.017±0.005	
	303.15K, 10bar	1.070±0.001	1.067 <sup>13,d</sup>	41.1±17.3		0.018±0.002	

<sup>a</sup> statistical uncertainties in units of the last digit displayed; <sup>b</sup> simulation; <sup>c</sup> experimental data; <sup>d</sup> at 303.05K, 1bar

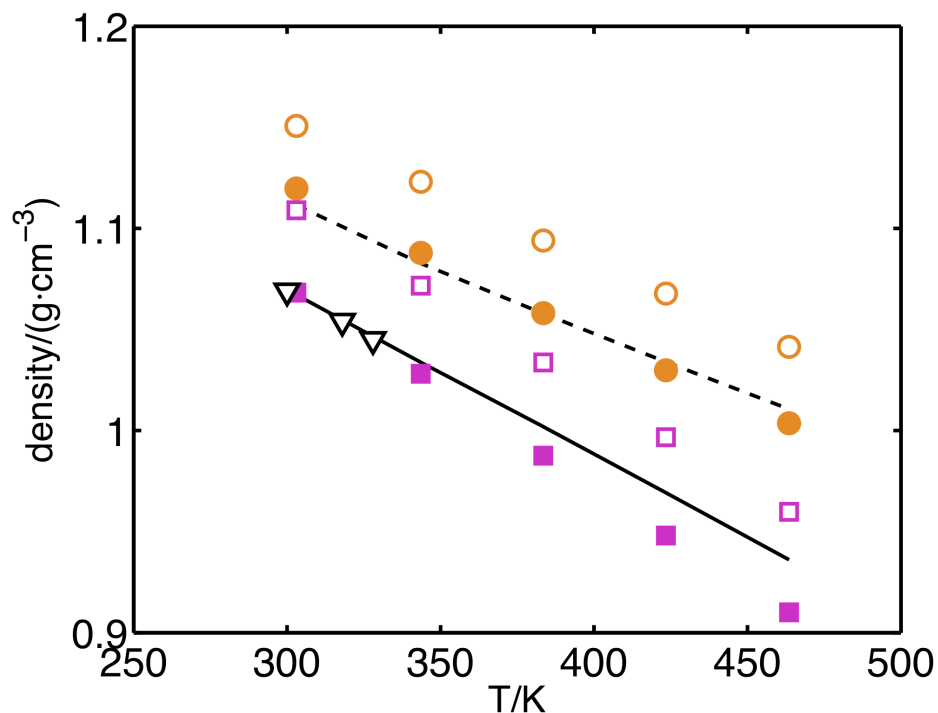


**Figure 1.** Density versus temperature for (EO)<sub>12</sub>DME. Filled squares: modified TraPPE at 0 bar; filled circles: modified TraPPE at 1000 bar; open squares: TraPPE at 0 bar; open circles: TraPPE at 1000 bar; continuous line: experimental data for PEODME ( $M_n \sim 600$ ,  $M_w/M_n = 1.06$ ) at 0 bar<sup>50</sup>; dashed line: experimental data for PEODME ( $M_n \sim 600$ ,  $M_w/M_n = 1.06$ ) at 1000 bar<sup>50</sup>; triangles: experimental data for ( $M_n \sim 398$ ,  $M_w/M_n = 1.16$ ) at 1 bar<sup>9</sup>.

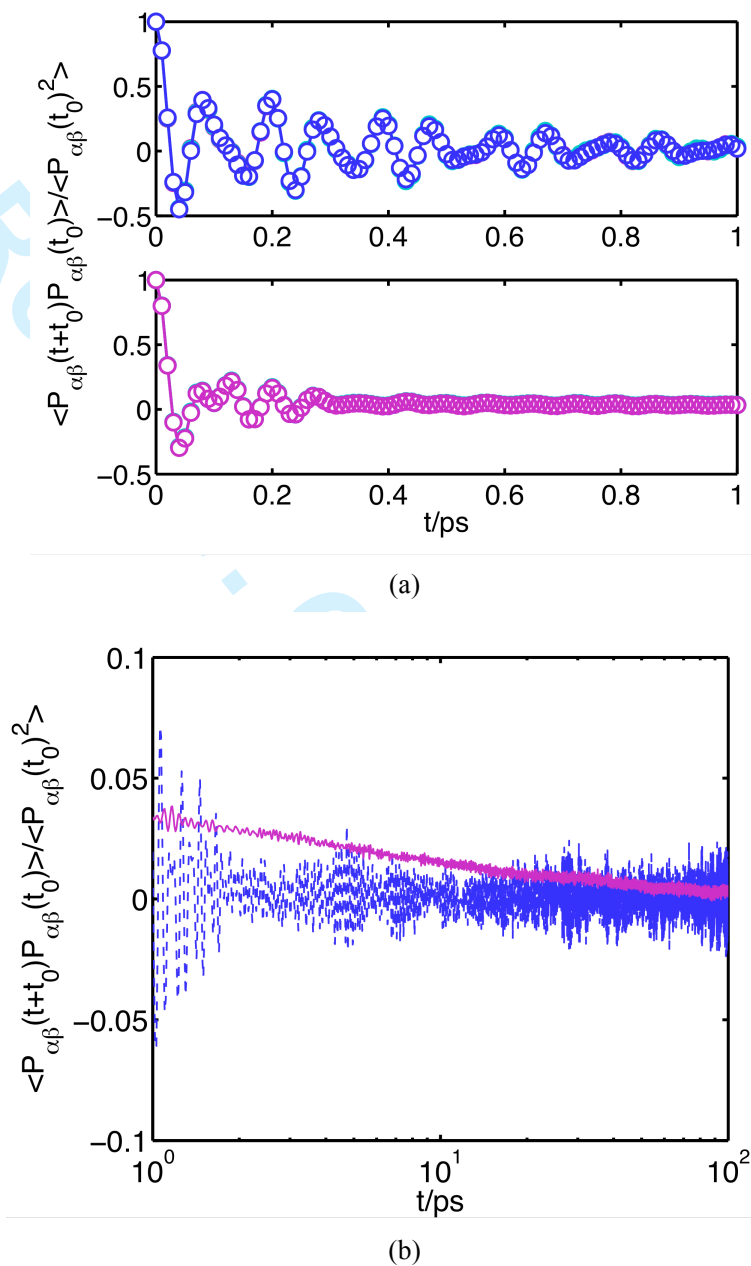
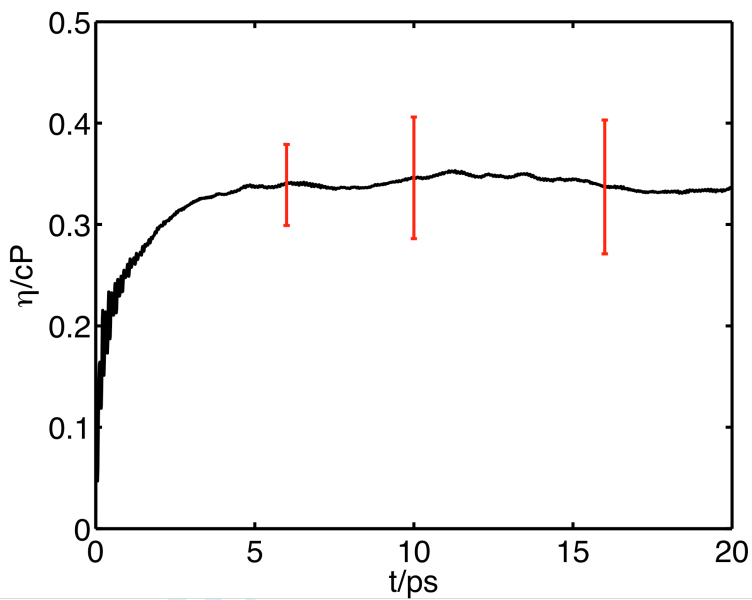
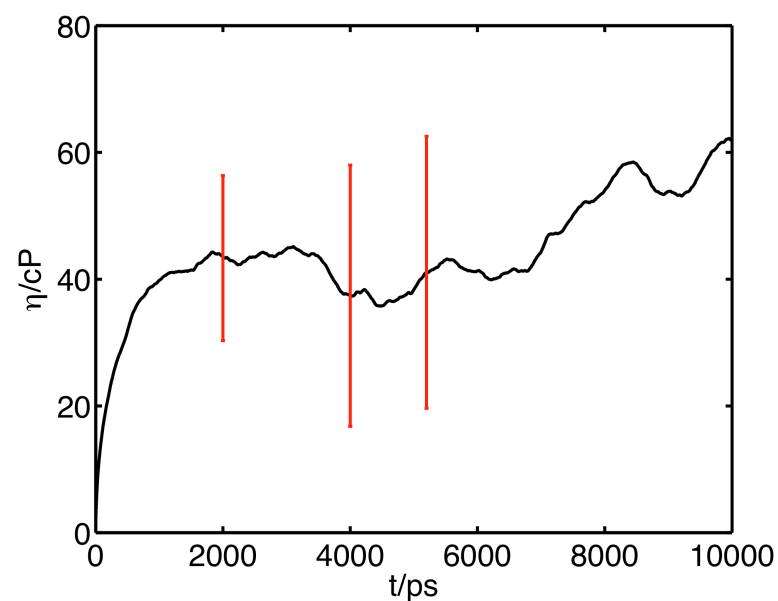


**Figure 2.** (a) Normalized autocorrelation functions of off-diagonal elements in the pressure tensors for DME (upper panel) and (EO)<sub>12</sub>DME; curves representing  $xy$ ,  $xz$ ,  $yz$  directions overlap quite well; (b) enlarged view of long-time tail of the pressure autocorrelation functions for DME (dashed line) and (EO)<sub>12</sub>DME (solid line).



(a)



(b)

**Figure 3.** Effective viscosities and their statistical uncertainties versus integration time for DME (top panel) and  $(EO)_{12}DME$  (bottom panel).

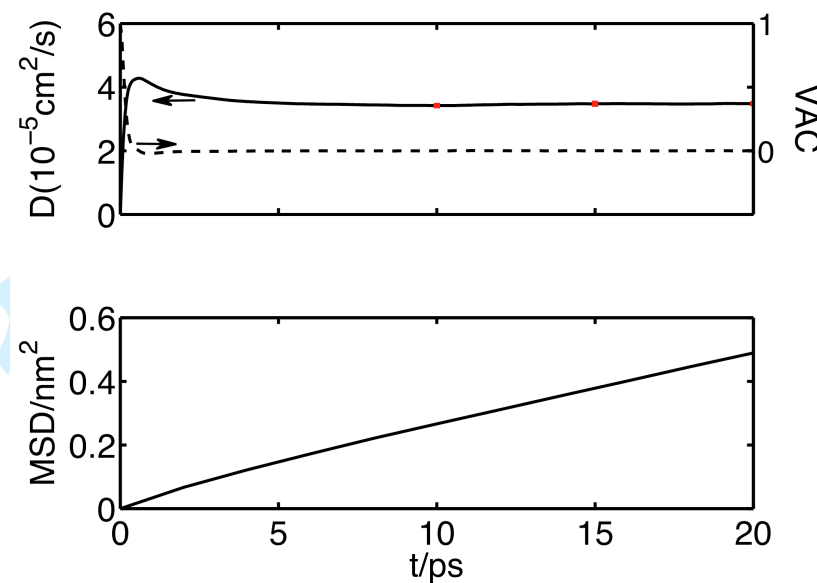


**Figure 4.** Calculation of self-diffusion coefficient of DME from GK integration (upper panel) and the MSD method (lower panel). The slope of the  $\text{MSD} \sim t$  fitted at 10 ~ 20ps is  $(3.45 \pm 0.03) \times 10^{-5} \text{ cm}^2/\text{s}$ .

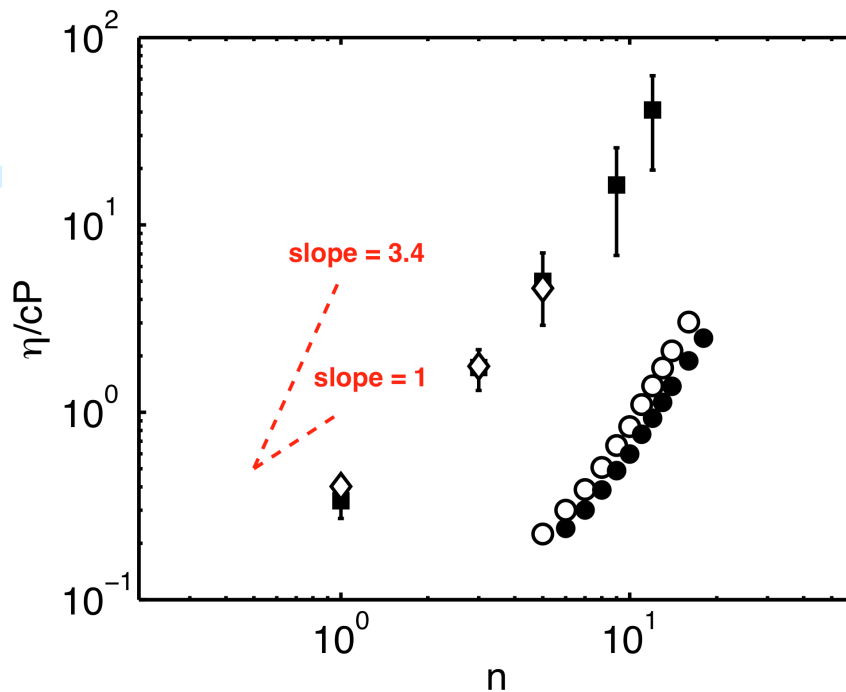


**Figure 5.** Chain length dependence of the shear viscosity. Solid squares: current simulations of  $\text{CH}_3\text{O}(\text{CH}_2\text{CH}_2\text{O})_n\text{CH}_3$  at 303.15K, 10bar; open diamonds: experiments of  $\text{CH}_3\text{O}(\text{CH}_2\text{CH}_2\text{O})_n\text{CH}_3$  at 303.15K, 10bar<sup>67</sup>; solid circles: experiments of *n*-alkanes at 298.15K, 1bar<sup>68</sup>; open circles: experiments of *n*-alkanes at 323.15K, 1bar<sup>68</sup>.

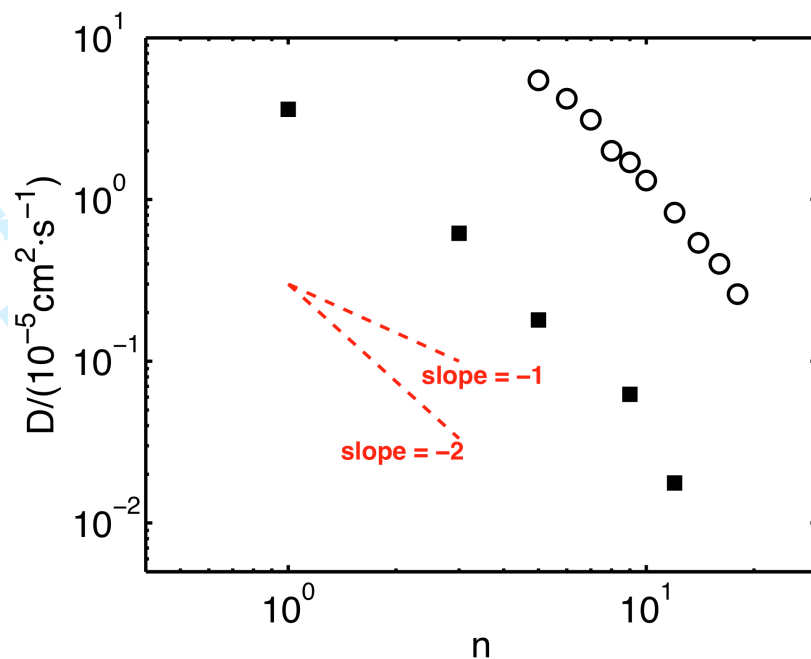


**Figure 6.** Chain length dependence of the self-diffusion coefficient. Solid squares: current simulations of  $\text{CH}_3\text{O}(\text{CH}_2\text{CH}_2\text{O})_n\text{CH}_3$  at 303.15K, 10bar; open circles: experiments of  $n$ -alkanes at 298.15K, 1bar<sup>69, 70</sup>

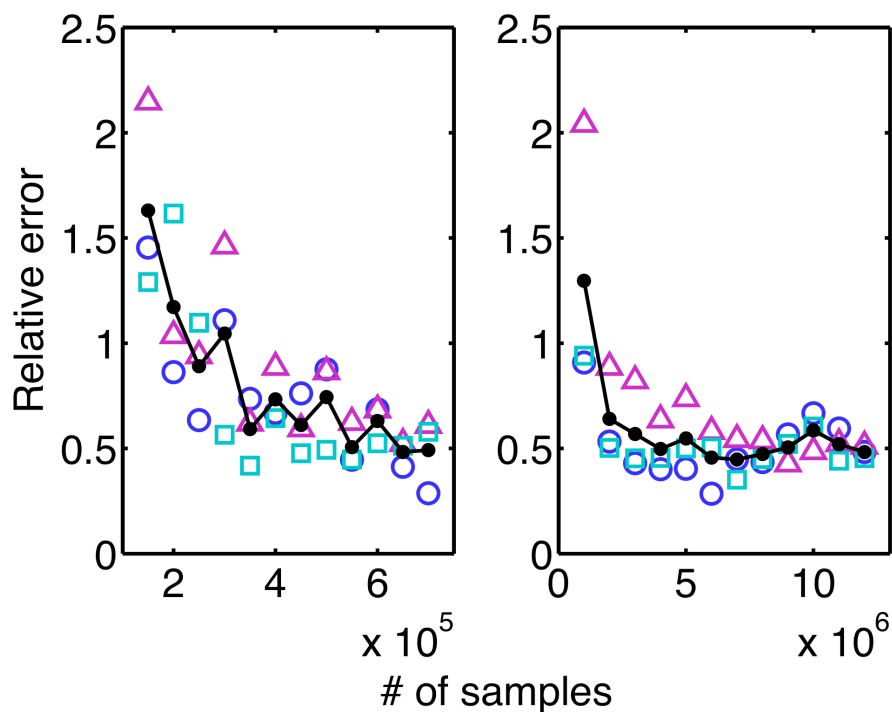


**Figure 7.** Relative errors of calculated viscosity vs. number of samples for (EO)<sub>5</sub>DME (left) and (EO)<sub>12</sub>DME (right) for an integration time of  $10\tau$ . Open circles, squares, and triangles represent the data from three independent runs at the same condition; solid line and solid circles are the average of the three runs.

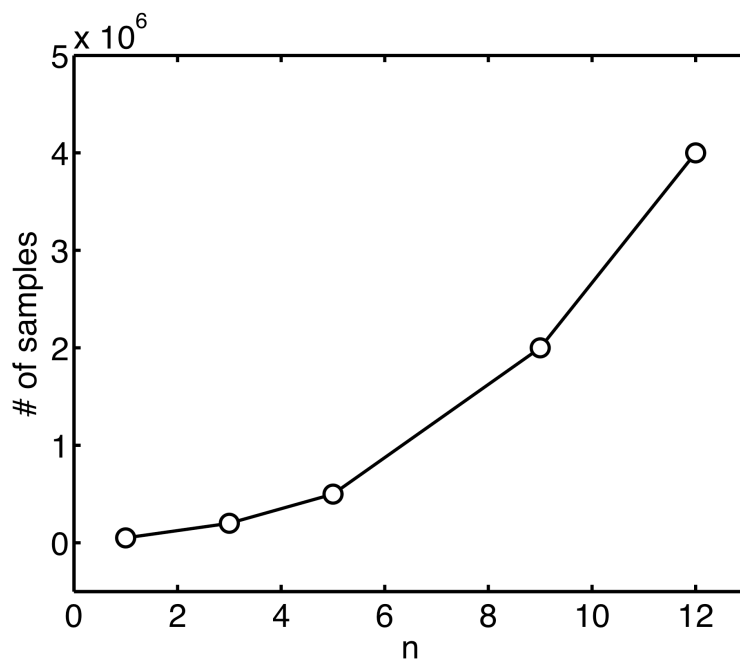


**Figure 8.** Number of samples required as a function of chain length. It reflects an approximate relation between the minimal production time and  $n$ .